Journal of Theoretical and Applied Mechanics, Sofia, Vol.54 (2024) pp. 201-215
SOLID MECHANICS

WAVE SCATTERING BY NANOINLCUSIONS IN ANISOTROPIC PLANE. PART II: NUMERICAL RESULTS

SONIA PARVANOVA[1]*, PETIA DINEVA[2]

[1]*Department of Structural Engineering,*
University of Architecture, Civil Engineering and Geodesy, Sofia, Bulgaria
[2]*Institute of Mechanics, Bulgarian Academy of Sciences, Sofia, Bulgaria*

[Received: 5 April 2023. Accepted: 11 May 2024]

doi: https://doi.org/10.55787/jtams.24.54.2.201

ABSTRACT: The mechanical model describing wave scattering by a system of elastic anisotropic nanoinclusions situated in an elastic anisotropic plane subjected to incident plane wave were considered in the first part of this work. The model is in the frame of 2D elastodynamics for general anisotropic continuum and surface elasticity theory proposed by Gurtin and Murdoch in 1975 [1]. The aim of the current part is to illustrate that the scattered wave field and stress concentration zones in an elastic generally anisotropic nanoheterogeneous plane is a complex result of mutual play of different key factors such as type and characteristics of the incident wave, surface elasticity properties, material anisotropy and dynamic interactions between nanoinclusions and between them and incident wave.

KEY WORDS: wave scattering, stress concentration, in-plane wave motion, anisotropic nanoinclusions, infinite anisotropic plane, BIEM, dynamic response in frequency and time domain.

1 PARAMETRIC STUDY

The current paper is continuation of the first part of this work. The importance of the presented chapter lies in the generality of the numerical methodology proposed in the first part of this work, and in the parametric study shown and discussed here. The simulation results reveal how the material anisotropy, the nanoinclusions existence, the wave parameters such as frequency and wave propagation direction, the surface elasticity effects appearing at nanolevel, the dynamic interaction between multiple inclusions and between them and the incident wave influence to the dynamic stress concentration distribution and to the scattered and diffracted wave field. The advantages of the proposed BIEM include all its important features as the reduction of the dimension of the problem, implicit satisfaction of the radiation condition at infinity,

*Corresponding author e-mail: slp_fce@uacg.bg

the semi-analytical character of the method, high solution accuracy of the problems considering stress concentration effects. In addition: (a) the method is valid for general type of anisotropy. It allows considering the cases, when the coordinate axes do not coincide with the axis of material symmetry; (b) the numerical procedure works for arbitrary incident wave angle, arbitrary geometry of the nanoinclusions shape and their mutual configuration.

Five different material models are considered in the parametric study and their material properties are given in Table 1.

Table 1: Material properties of different materials used in the parametric study

Mat. type	Stiffness tensor components, [MPa]	ρ [t/m^3]
MatType 1	$c_{11} = 43.952;\quad c_{12} = 17.952;\quad c_{22} = 43.952;\quad c_{66} = 13$	2.8
MatType 2	$c_{11} = 81.4505;\quad c_{12} = 17.952;\quad c_{22} = 42.79225;\quad c_{66} = 13$	2.8
MatType 3	$c_{11} = 118.949;\quad c_{12} = 17.952;\quad c_{22} = 41.6325;\quad c_{66} = 13$	2.8
MatType 4	$c_{11} = 156.4475;\quad c_{12} = 17.952;\quad c_{22} = 40.47275;\quad c_{66} = 13$	2.8
MatType 5	$c_{11} = 193.946;\quad c_{12} = 17.952;\quad c_{22} = 39.313;\quad c_{66} = 13$	2.8

The three materials MatType 2, MatType 3 and MatType 4 are chosen between the following limit cases: (a) LiNaKCsPO3 Glass Fiber denoted as MatType 5 ($c_{11} = 193.946$; $c_{12} = 17.952$; $c_{22} = 39.313$; $c_{66} = 13$ MPa), the material properties are introduced in [2], and (b) equivalent isotropic matrix material (MatType 1) with Lame constants $\lambda = c_{12} = 17.952$ MPa and $\mu = c_{66} = 13$ MPa corresponding to the anisotropic one as far as the stiffness coefficients c_{12} and c_{66} are equal. The stiffness tensor of the equivalent isotropic material is then defined as: $c_{11} = c_{22} = \lambda + 2\mu = 43.952$ MPa, $c_{12} = 17.952$ MPa, $c_{66} = 13$ MPa. The difference between MatType 5 and its isotropic equivalent MatType 1 is only in c_{11} and c_{22} stiffness components. Note that three intermediate matrix materials MatType 2, MatType 3 and MatType 4 are with c_{11} and c_{22} stiffness components linearly interpolated between both the limit states. The inclusion stiffness tensor is assumed 10 times softer than the respective matrix tensor in all the models under consideration, the inclusion density is assumed $\rho_I = 1$ t/m^3.

The proposed model allows arbitrary shape of all the nanoinclusions, however just for the aim of illustration a circular nanoinclusion with radius $a_0 = 10^{-9}$ m is considered. It is assumed that the surface elastic constants λ_s, μ_s for all interfaces are one and the same and $\alpha^S = \lambda^S + 2\mu^S$ is in the neighborhood of ± 10 N/m, see Tian and Rajapakse [3]. The residual surface tension τ_0 is ignored in the dynamic analyses.

The following non-dimensional parameters are used in the parametric study: (a)

non-dimensional frequency $\Omega = kd = \omega 2a_0/\sqrt{c_{66,M}/\rho_M}$ where ω is frequency of the incident wave and d is the diameter of the inclusion; (b) non-dimensional time duration $\tau = (t/a_0)\sqrt{c_{66,M}/\rho_M}$; (c) normalized surface elasticity coefficient $s = \alpha^s/(2a_0 c_{66,M})$; (d) normalized dynamic stress concentration factor (DSCF) defined as DSCF $= \sigma_{\varphi\varphi}/\sigma_0$, where $\sigma_{\varphi\varphi}$ is the hoop or circumferential stress, normalized by the incident stress σ_0 defined as $\sigma_0 = -\mu_M u_0(\omega/C_{SV,M})^2$, where u_0 is the unit amplitude of the incident wave, $C_{SV,M}$ is the shear wave velocity of the elastic matrix; (e) normalized displacement components u_i/u_0, i =1,2. Note that in the time-domain analysis the displacements are normalized again by u_0 and the hoop stresses by σ_0 as in frequency domain. The location of the observer point is defined by the polar angle φ. In all the parametric examples bellow the inclusion-matrix interface is modelled by 32 quadratic boundary elements. The frequency range is up to dimensionless frequency $\Omega = 12$, divided to 50 equal frequency steps. For the results in time domain the frequency range is extended to $\Omega = 16$ divided to 800 equal frequency steps.

The dynamic time-harmonic or transient excitation is presented by horizontally propagating incident plane waves referred as quasi P- (qP) and quasi SV- (qSV) waves as far as they are not purely longitudinal and purely transversal in anisotropic medium, see Kerner et al. [4]. DSCFs measured at fixed observer points $\varphi = \pi/2$ and $\varphi = \pi/4$, correspondingly, versus normalized frequency Ω of the horizontally propagating qP-waves and qSV-waves, for all the materials defined in Table 1, are depicted in Fig. 1. The surface elasticity effect is not considered in these plots.

Figure 2 shows normalized displacement components versus dimensionless frequency for the same materials at observer points $\varphi = 0;\ \pi/2$ due to horizontally

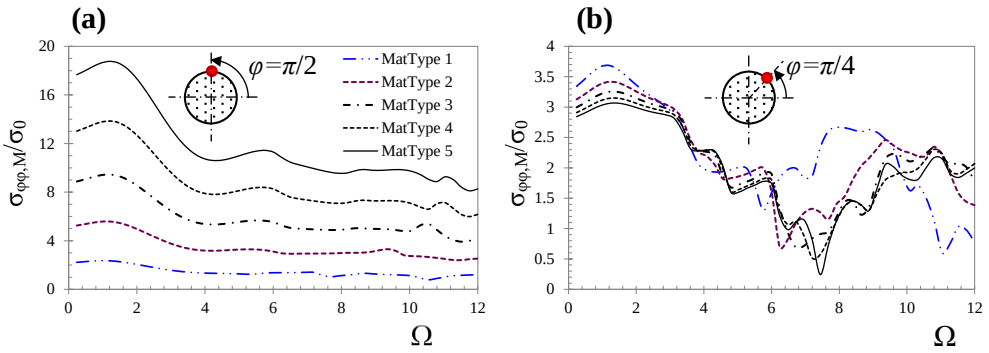

Fig. 1: Normalized hoop stresses at marked observer point from the matrix side versus dimensionless frequency of the horizontally propagating plane waves for different material type: (a) qP-waves; (b) qSV-waves.

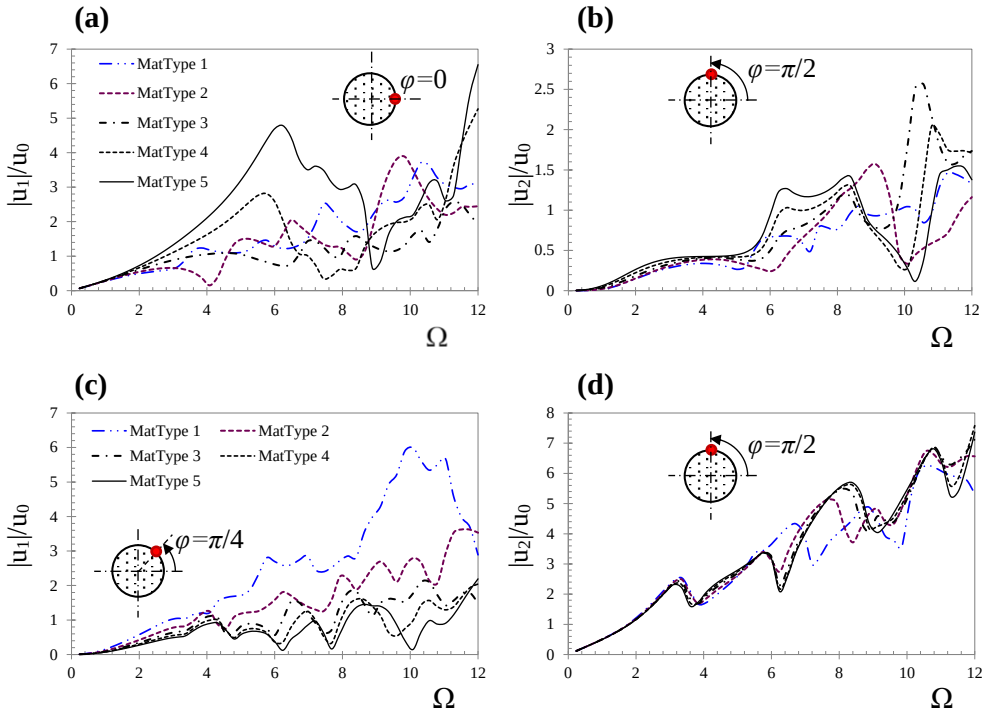

Fig. 2: Normalized displacement components for different material types at marked observer points versus dimensionless frequency of the horizontally propagating waves: (a,b) qP-waves; (c,d) qSV-waves.

propagating qP-waves and at observer points $\varphi = \pi/4;\ \varphi = \pi/2$ in the case of horizontal qSV-waves. The strong influence of the material anisotropy on the DSCF is clearly illustrated in Fig. 1a for the observer point $\varphi = \pi/2$. The maximal stress concentration values occur at the anisotropic material MatType 5 and they decrease with decreasing of the stiffness coefficients and become minimal for the isotropic material MatType 1. The peak values for all the materials are happened at $\Omega = 1.2$ and they are not changed for the different materials. The maximal hoop stress at frequency $\Omega = 1.2$ for MatType 5 is 8 times larger than the corresponding stress magnitude for MatType 1 material. The tendency is just in opposite in the case of incident SV wave, see Fig. 1b and Fig. 2c for the observer point $\varphi = \pi/4$, where the maximal dynamic response values occur for elastic isotropic material MatType 1.

The conclusion is that the material anisotropy plays a crucial role for dynamic behaviour of the object under consideration, of course, together with the additional factors such as the type of the incident wave, its frequency and propagation direction and also the position of the observer point.

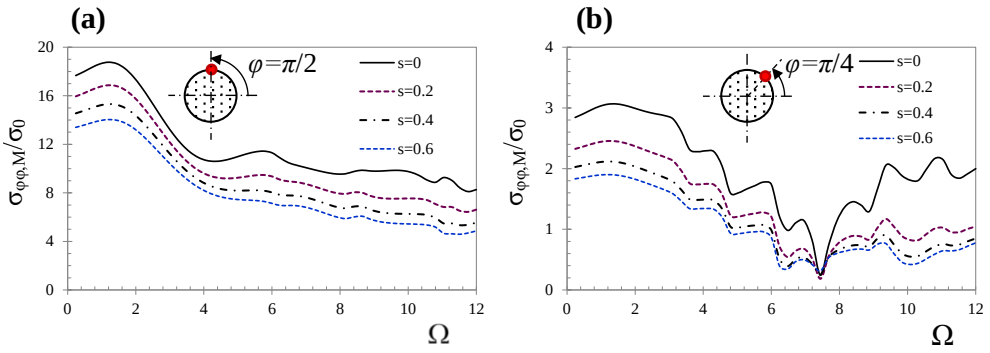

Fig. 3: Normalized hoop stresses at marked observer point from the matrix side for LiNaKCsPO3 Glass Fiber versus dimensionless frequency of the horizontally propagating waves at variable surface parameter s: (a) qP-wave; (b) qSV-wave.

Figures 3 and 4 reveal the sensitivity of the frequency-dependent wave field to the surface elasticity effects. Normalized hoop stresses for matrix made of LiNaKCsPO3 Glass Fiber versus dimensionless frequency Ω of the horizontally propagating qP-waves and qSV-waves and for different surface parameter s are given in Figs. 3a,b for fixed observer points from the matrix side. The following effect is visible: as the surface parameter s values increases, the DSCF values invariably drop, which indicates that strong molecular surface action overrides the classical mechanical effects observed at the macroscale. This tendency is clearly pronounced for both types of waves. Again, the specific character of the wave pictures is sensitive to the observer point position and to the type, frequency and propagation direction of the excitation load.

Figure 4 draw normalized displacement components at the fixed observer points for matrix made of LiNaKCsPO3 Glass Fiber and variable surface parameter versus dimensionless frequency of the horizontally propagating P-waves (Figs. 4a,b) and SV-waves (Figs. 4c,d). The trend from Fig. 3 discussed above is not clearly shown here in Fig. 4. It can be seen in Fig. 4c that with increasing the surface elasticity parameter s, the displacement values also increase in the frequency interval under consideration. The conclusion is that the scattered, diffraction and stress concentration wave field is a complex result of mutual play of many different factors such as type of the dynamic load and its characteristics, type of the material anisotropy, type of the surface elasticity coefficients, and also the location of the observer point.

During their operational life, nanostructures may be exposed to suddenly applied mechanical loads with very short duration time and they experience transient vibrations within this time. To the author's best knowledge, the transient response analy-

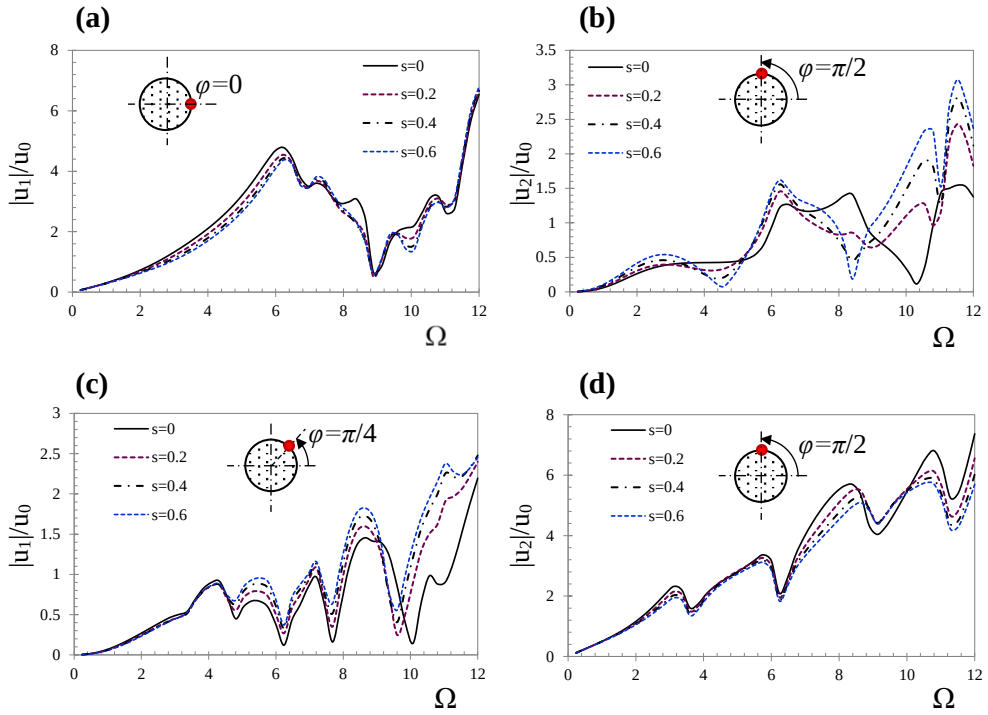

Fig. 4: Normalized displacement components at fixed observer points for matrix made of LiNaKCsPO3 Glass Fiber and variable surface parameter s versus dimensionless frequency Ω of horizontally propagating wave: (a,b) qP-waves; (c,d) qSV-waves.

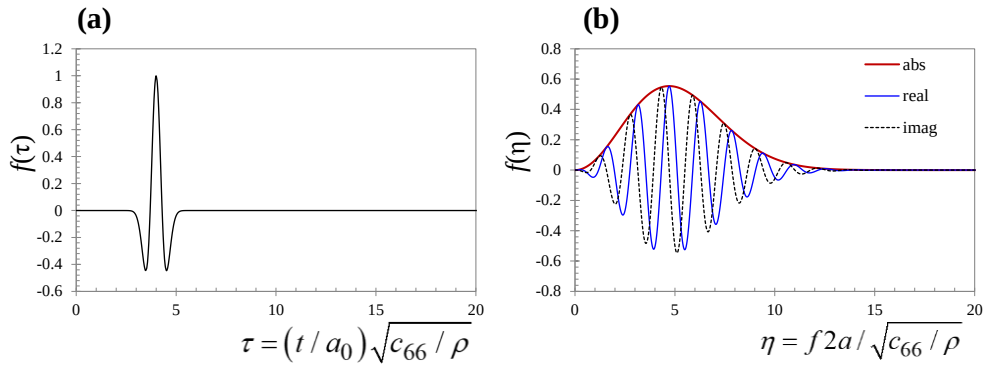

Fig. 5: Time-history function and its Fourier transform.

sis in nanomechanics based on surface elasticity theory is a novel topic which is not studied before. The knowledge of dynamic time-dependent behavior of nanoscale structures containing nanoinclusions is important as far as transient impulsive type of loads during the fabrication and service conditions exist. Both analyses in frequency and time domain have their own importance. What follows is to discuss some solutions obtained in time-domain as a result of an applied transient impulse load, shown in Fig. 5. The incident P/SV waves are transient ones with time function depicted in Fig. 5a and amplitude-frequency characteristic given in Fig. 5b. The time domain results are obtained from frequency domain results by using descrete Inverse Fast Fourier Transform (IFFT) algorithm. The time function is the well-known Ricker wavelet defined as:

$$f(\tau) = \left(1 - 2\pi^2\eta_c^2(\tau - \tau_0)^2\right)\exp\left(-\pi^2\eta_c^2(\tau - \tau_0)^2\right) \quad \text{or}$$
$$f(t) = \left(1 - 2\pi^2 f_c^2(t - t_0)^2\right)\exp\left(-\pi^2 f_c^2(t - t_0)^2\right).$$

Here $\eta_c = \omega_c a_0 / \left(\pi\sqrt{c_{66,M}/\rho_M}\right)$ or $\eta_c = f_c 2a_0 / \left(\sqrt{c_{66,M}/\rho_M}\right)$ is the normalized characteristic dimensionless frequency, f_c is characteristic frequency in Hz, $\tau = (t/a_0)\sqrt{c_{66,M}/\rho_M}$ is the normalized time. Note that $\eta_c\tau = f_c t$ and for the time function is valid $f(\tau) = f(t)$. In all the calculations η_c is set to 0.75 and the normalized time τ_0 is set to 4. The frequency range in the analysis is divided into 200 equal frequency steps.

Figures 6 and 7 illustrate the influence of the material anisotropy to the time-dependent DSCF and scattered displacement field in an elastic anisotropic plane with a circular elastic anisotropic nanoinclusion having stiffness tensor 10 times softer than the respective matrix tensor. Normalized hoop stresses for the material type

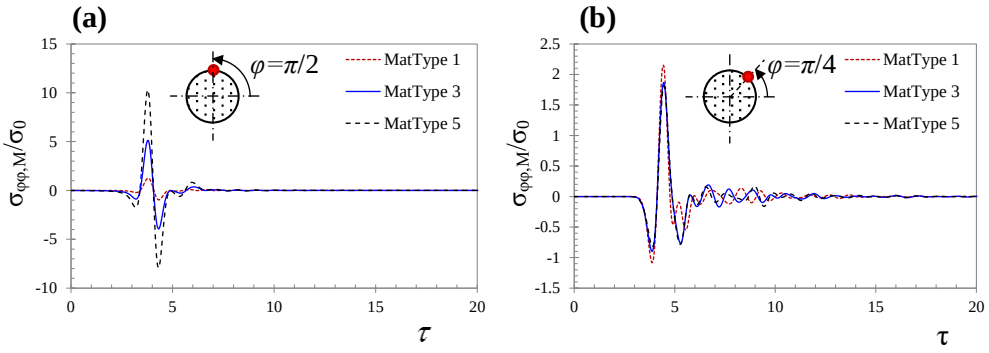

Fig. 6: Normalized hoop stresses at marked observer point from the matrix side for variable material type versus dimensionless time, due to horizontally propagating transient wave: (a) qP-waves; (b) qSV-waves.

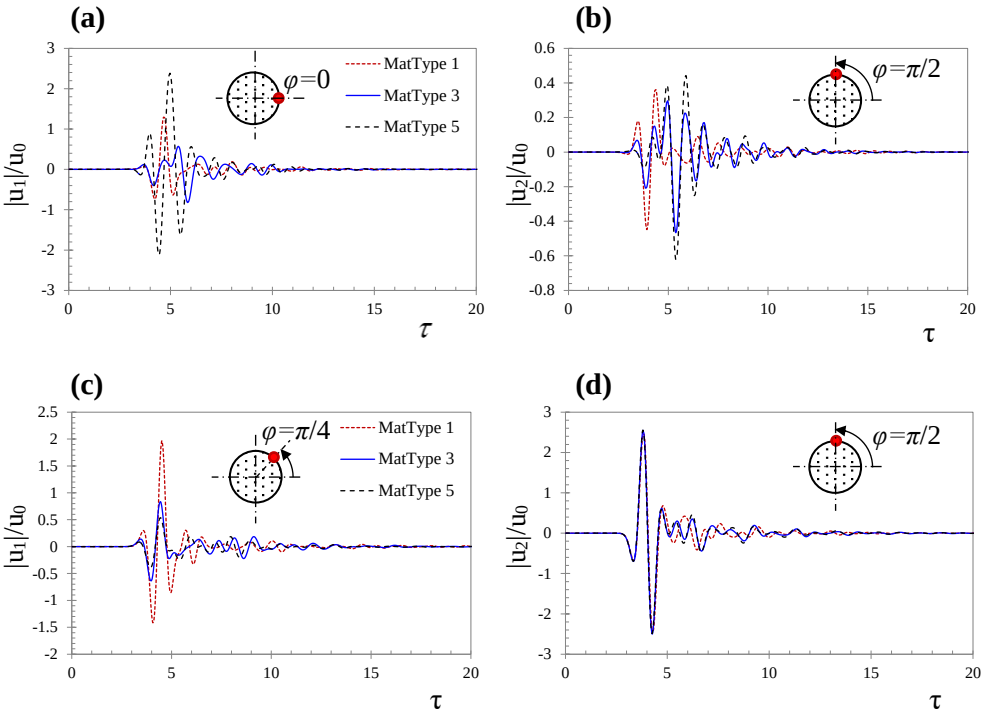

Fig. 7: Normalized displacement components at marked observer points for different material types versus dimensionless time due to horizontally propagating (a,b) qP-waves; (c,d) qSV-waves.

in Table 1 versus dimensionless time at fixed observer points from the matrix side due to horizontally propagating transient qP and qSV wave is presented in Fig. 6. Figure 7 shows normalized displacement components for the same material types at different observer points versus dimensionless time due to horizontally propagating transient longitudinal and shear wave. The maximal peak values of the DSCF belong to the observer point $\varphi = \pi/2$ for anisotropic material MatType 5 in the case of incident qP-wave, Fig. 6a. However, Fig. 6b reveals that the peak values for DSCF occur for elastic isotropic material in the case of incident SV wave at the observer point $\varphi = \pi/4$. The frequency of the peak values do not change for the different materials. Figure 7 confirms the above discussed tendency that in the case of incident qP-wave the maximal response occurs for MatType 5 material, see Figs. 7a-b, while the maximal displacement response is realized for linear elastic material MatType 1 in the case of incident transient qSV wave, see Figs. 7c-d. All the results in Figs. 6 and 7 are for the absence of surface elasticity effect.

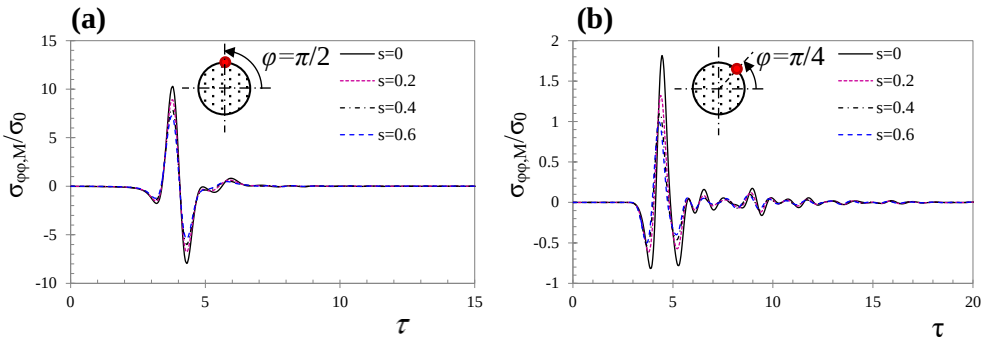

Fig. 8: Normalized hoop stresses for matrix made of LiNaKCsPO3 Glass Fiber versus dimensionless time and variable surface parameter s, at marked observer point from the matrix side, due to horizontally propagating (a) qP-waves; (b) qSV-waves.

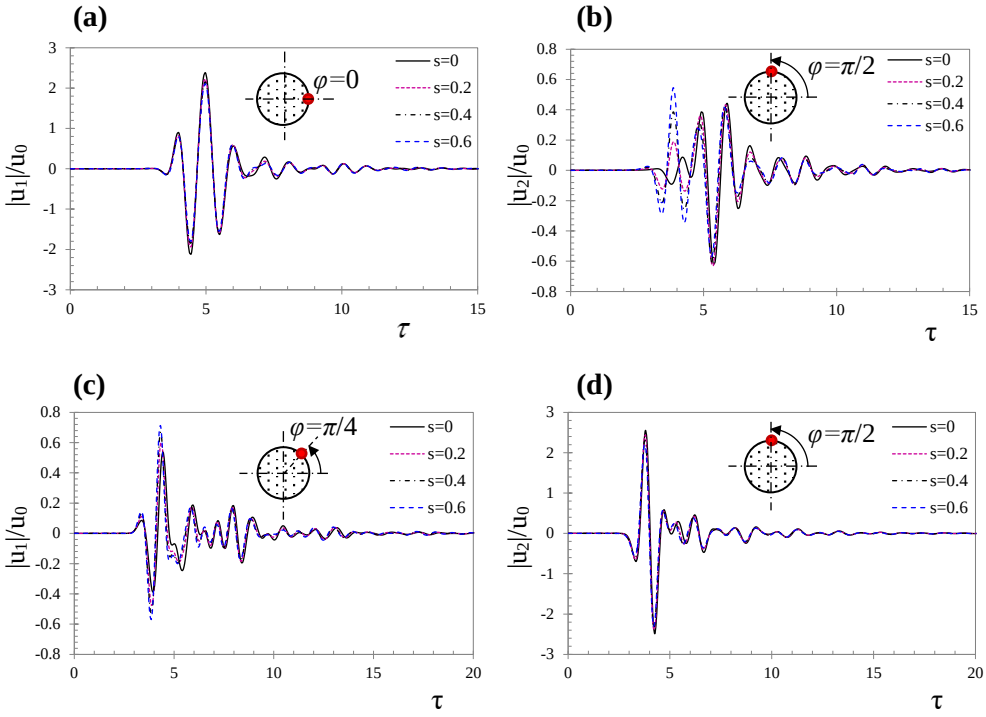

Fig. 9: Normalized displacement components at marked observer points for matrix made of LiNaKCsPO3 Glass Fiber at variable surface parameter s versus dimensionless time due to horizontally propagating (a,b) qP-waves; (c,d) qSV-waves.

Figures 8 and 9 show the surface elasticity effects on the transient wave field due to incident P and SV wave. Normalized hoop stresses and normalized displacement components at fixed observer points along interface boundary for matrix made of LiNaKCsPO3 Glass Fiber versus dimensionless time and for different surface parameter s are depicted in Figs. 8-9 respectively. The same tendency to decrease the dynamic response with increase of the surface elasticity parameter is observed, except the case shown in Fig. 9c concerning the normalized horizontal displacement at point $\varphi = \pi/4$ in the case of incident SV wave.

DSCFs along the whole matrix-inclusion interface, versus normalized frequency Ω of the horizontally propagating qP-waves and qSV-waves, for LiNaKCsPO3 Glass Fiber and surface elasticity parameter $s = \alpha^s/(2a_0c_{66,M}) = 0.2$ are portrayed in

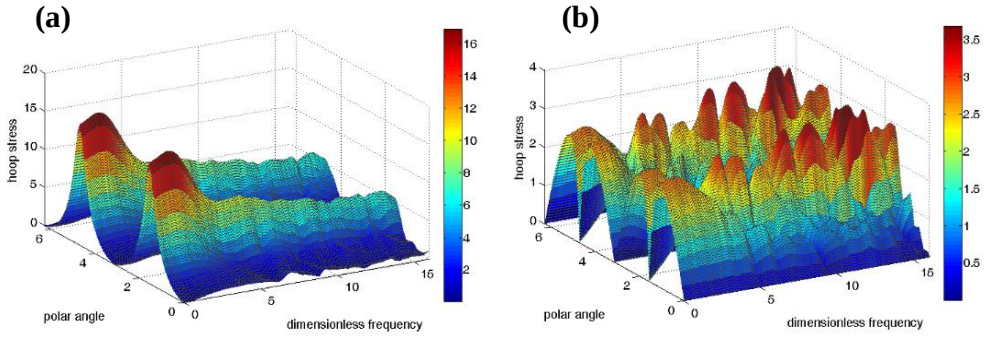

Fig. 10: Normalized hoop stresses along the contact interface from the matrix side for LiNaKCsPO3 Glass Fiber versus dimensionless frequency of the horizontally propagating waves for surface parameter $s = 0.2$: (a) qP-wave; (b) qSV-wave.

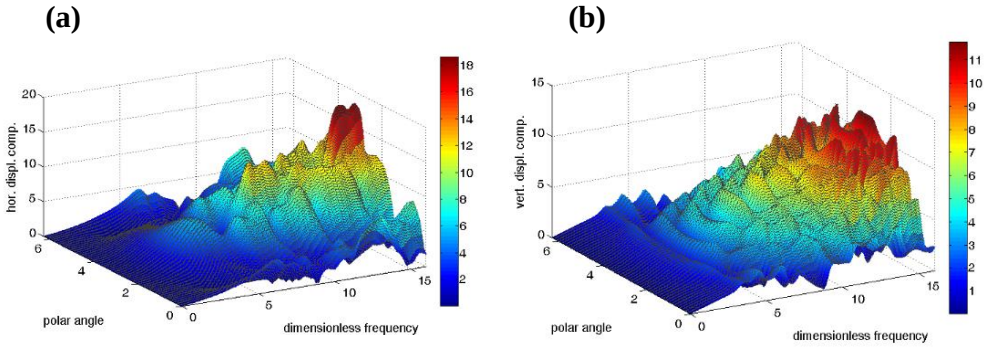

Fig. 11: Normalized displacement components at the contact interface for LiNaKCsPO3 Glass Fiber versus dimensionless frequency, for surface parameter $s = 0.2$, caused by horizontally propagating: (a) qP-wave ($|u_1/u_0|$); (b) qSV-wave ($|u_2/u_0|$).

Figs. 10a,b. The plotted hoop stresses are from matrix side. Figures 11a,b show the normalized horizontal displacement components and normalized vertical displacement components along the whole contact interface due to horizontally propagating qP- and qSV- waves.

The same set of results but in time domain are illustrated in Figs. 12 and 13. The normalized hoop stresses along the contact interface versus dimensionless time from the matrix side, for horizontally propagating qP- and qSV- waves, are shown in Fig. 12. The respective displacement components along the contact interface versus normalized time are given in Fig. 13. In all 3D figures the surface elasticity parameter is set to 0.2.

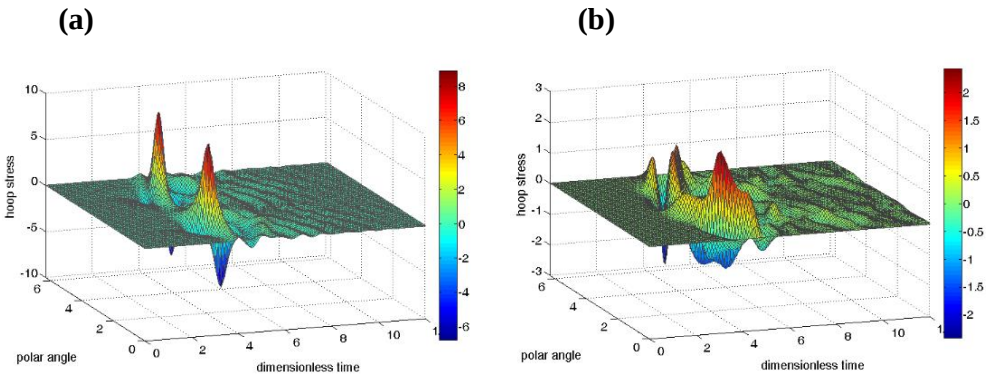

Fig. 12: Normalized hoop stresses along the contact interface from the matrix side for LiNaKCsPO3 Glass Fiber versus dimensionless time of the horizontally propagating waves for surface parameter $s = 0.2$: (a) qP-wave; (b) qSV-wave.

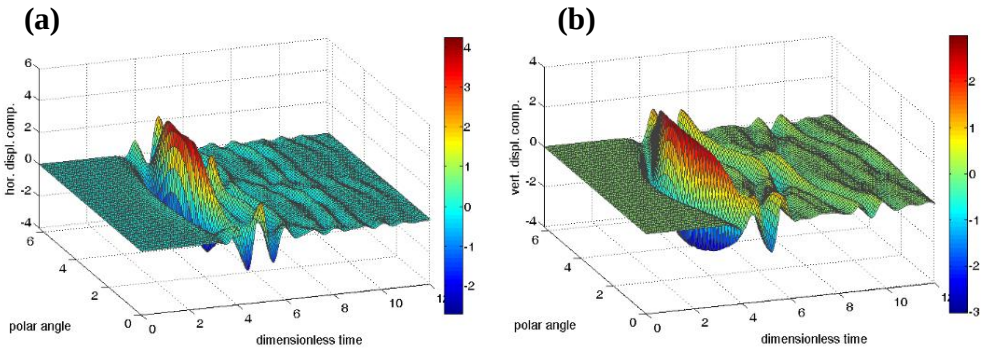

Fig. 13: Normalized displacement components at the contact interface for LiNaKCsPO3 Glass Fiber versus dimensionless frequency, for surface parameter $s = 0.2$, caused by horizontally propagating: (a) qP-wave (u_1); (b) qSV-wave (u_2).

The sensitivity of the scattered, diffracted and dynamic local stress concentration fields to the following key model parameters are studied in our parametric analysis in both frequency and time domain hitherto: (a) the type and properties of the incident wave; (b) the observer point position; (c) the type and properties of the material anisotropy; (c) the inclusion size and surface elasticity properties. The mechanical model proposed in Part I consider arbitrary number of the anisotropic inclusions and in addition their arbitrary geometrical configuration in an anisotropic plane.

The next two Figs. 14–15 present dynamic response of three anisotropic nanoinclusions ordered in a horizontal line in an anisotropic infinite continuum and subjected to horizontally propagating longitudinal qP-wave. Different anisotropic materials are compared, and they are of the following types: elastic isotropic material named as MatType 1, MatType 3 and MatType 5 with material properties presented in Table 1. The distance between nanoinclusions is $2.5a_0$. The stress concentration fac-

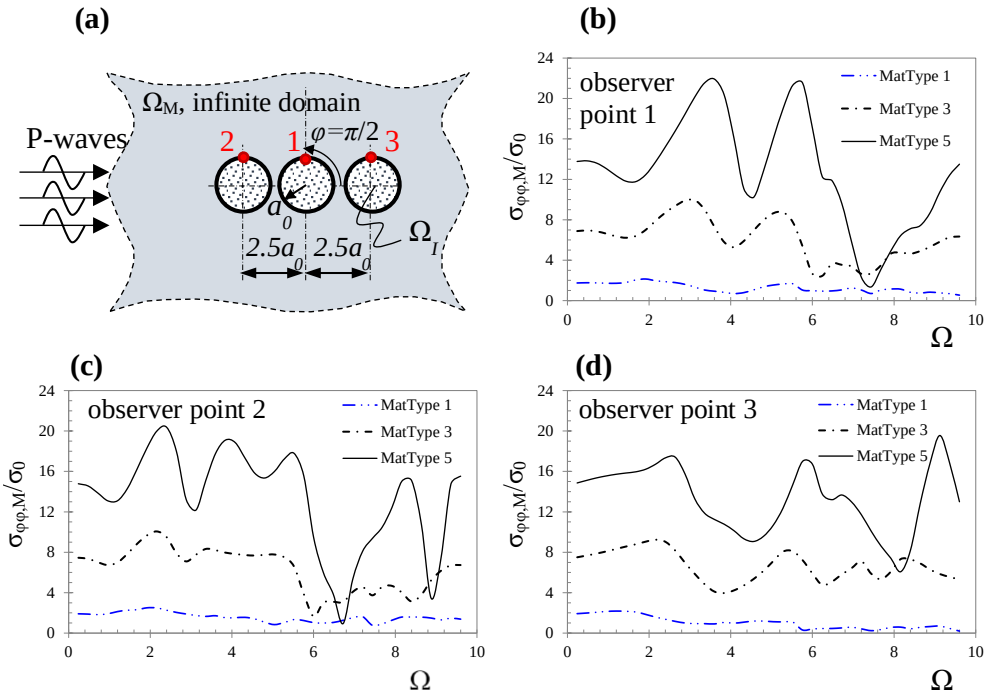

Fig. 14: Normalized hoop stresses at marked observer points from the matrix side versus dimensionless frequency of the horizontally propagating plane qP-waves for different material type and s =0: (a) problem geometry; (b) $\varphi = \pi/2$, central inclusion; (c) $\varphi = \pi/2$, left inclusion; (b) $\varphi = \pi/2$, right inclusion.

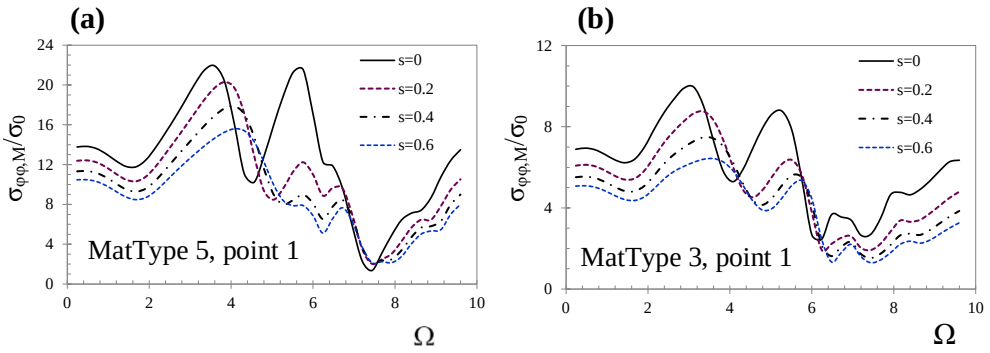

Fig. 15: Normalized hoop stresses at central inclusion for polar angle $\varphi = \pi/2$ from the matrix side versus dimensionless frequency of the horizontally propagating qP-waves at variable surface parameter s for: (a) LiNaKCsPO3 Glass Fiber; (b) MatType 3.

tors are measured at three different observer points with one and the same polar angle $\varphi = \pi/2$ but on the central, left and right nanoinclusion, see Fig. 14a. Figures 14b,c,d draw normalized hoop stresses at marked observer points from the matrix side versus dimensionless frequency without taking into consideration the surface elasticity influence, i.e. for s =0. The strong influence of the material anisotropy is evident and in addition the dynamic interaction between all the three nanoinclusions is clearly illustrated. The stress concentration effects are much greater for anisotropic material MatType 5 and the frequencies where the maximal and minimal SCFs values occur are different for the three materials. The differences between maximal SCF at Ω =1.92 for MatType 1 (elastic isotropic case), and maximal SCF at Ω =3.6 for MatType 5 are as follows: (a) for observer point 1 the DSCF is 10.3 times larger in case of anisotropic material; (b) for observer point 2 the same ratio is 7.1; (c) for observer point 3 it is 6.1. Figures 15a,b show normalized hoop stresses at central inclusion for polar angle $\varphi = \pi/2$ from the matrix side versus dimensionless frequency of the horizontally propagating qP-waves at different variable surface parameters s for different anisotropic materials-LiNaKCsPO3 Glass Fiber and MatType 3. The hybrid influence of both model parameters - the material anisotropy and the surface elasticity on the nonuniform dynamic stress distribution near the nanoinclusion is clearly demonstrated in Fig. 15. The following general trend is maintained: (a) the dynamic response decreases with increase of the surface elasticity parameter; (b) the dynamic response increases with increase of the stiffness coefficients of the anisotropic material.

The presented above numerical results show that both the wave-nanoinclusion

interaction and the dynamic interaction between multiple nanoinclusions in an elastic anisotropic plane depend on the combined influence of the incidence wave type, its direction and frequency, of the number and geometrical configuration of nanoinclusions, of the ratio of the wave length to the inclusion size, of the type of material anisotropy and of the surface elasticity phenomenon. The developed mechanical model, accompanied numerical scheme and the verified program codes have the potential to be used as a base for solution of dynamic anisotropic problems in nanomechanics with more complex geometrical and mechanical properties.

2 CONCLUSIONS

The innovation point in the proposed work is development of a numerical model and verified numerical scheme based on the BEM for solution of anisotropic elastodynamic problem in nanomechanics. Both are inserted in detail parametric study describing scattered and stress concentration wave fields in anisotropic solid with multiple anisotropic nano-inclusions subjected to time-harmonic and transient dynamic loadings. To the authors' best knowledge there are no available results for the problem under consideration. The presence of nano-inclusions reveals additional effects comparing with the case of nano-cavities, and this is illustrated in the presented parametric study.

More specifically, the in-plane wave motion in the frequency and time domain is studied for an infinite heterogeneous elastic anisotropic matrix containing multiple elastic anisotropic nanoinclusions. A combination of a direct and inverse FFT and a direct sub-structuring BEM formulation is developed, employing fundamental solutions of the Navier-Cauchy equations of dynamic equilibrium for the bulk elastic generally anisotropic solid. The BEM formulation is augmented by the Gurtin–Murdoch [1] surface elasticity model, which accounts for the correct boundary conditions for displacements and tractions along all surfaces when the problem is solved at the nanoscale. The model and the accompanied numerical scheme, together with a detail verification study is presented in Part-I.

Numerical simulations presented in this second part are performed for computation of the DSCF which develops around nanoinclusions and for evaluation of the scattered and diffraction wave field in an elastic anisotropic nanoheterogeneous matrix in order to help clarify their mechanical behaviour and to establish the relative importance of the geometric, material and load parameters of the problem. The numerical results obtained in frequency and time domain show a marked dependence of the non-uniform stress and displacement fields to the size of the nanoinclusions presented by the normalized surface elasticity coefficient, to their number and position, as well as to their mutual interaction with the incoming elastic waves propagating in infinite anisotropic solids.

The numerical simulations demonstrate the potential of the BIEM to produce highly accurate results regarding the dynamic behaviour of anisotropic materials strengthened (or weakened) by multiple elastic and anisotropic nanoinclusions, with marked economy as compared to the standard engineering analysis employing domain-based techniques such as finite elements and finite differences.

The present work in two-parts serves as a spring board for solving more complex nanomechanical problems involving nanocomposites and structural nanoelements containing different types of heterogeneities such as cracks, pores, fibres, layers and materials with nanorelief pequliarities.

ACKNOWLEDGMENT

The first author wishes to acknowledge support provided by the Research, Consultancy and Design Centre (RCDC) of UACEG-Sofia through Grant No. БН-298/24. The second author is supported by the Bulgarian National Science Fund, contract No. КП-06-Н57/3/15.11.2021.

REFERENCES

[1] M.E. GURTIN, A.I. MURDOCH (1975) A continuum theory of elastic material surfaces. *Archive for Rational Mechanics and Analysis* **57** 291-323.

[2] J. ENDO, S. INABA, S. ITO (2015) Mechanical properties of anisotropic metaphosphate glass. *Journal of the American Ceramic Society* **98**(9) 2767-2771.

[3] L. TIAN, R.K.N.D. RAJAPAKSE (2007) Elastic field of an isotropic matrix with a nanoscale elliptical inhomogeneity. *International Journal of Solids and Structures* **44** 7988-8005.

[4] C. KERNER, B. DYER, M. WORTHINGTON (1989) Wave propagation in a vertical transversely isotropic medium: field experiment and model study. *Geophysical Journal International* **97**(2) 295-309.